RSC Advances

PAPER

View Article Online
View Journal | View Issue

Cite this: *RSC Adv.*, 2021, **11**, 39888

Theoretical study on molecular mechanism of aerobic oxidation of 5-hydroxymethylfurfural to 2,5-diformyfuran catalyzed by VO_2^+ with counterpart anion in *N*,*N*-dimethylacetamide solution†

Zhen-Bing Si,[a] Jin-Shan Xiong,[a] Ting Qi,[a] Hong-Mei Yang,[a] Han-Yun Min,[a] Hua-Qing Yang *[a] and Chang-Wei Hu[b]

Received 30th September 2021
Accepted 3rd December 2021

DOI: 10.1039/d1ra07297h

rsc.li/rsc-advances

Vanadium-containing catalysts exhibit good catalytic activity toward the aerobic oxidation of 5-hydroxymethylfurfural (HMF) to 2,5-diformyfuran (DFF). The aerobic oxidation mechanism of HMF to DFF catalyzed by VO_2^+ with counterpart anion in *N*,*N*-dimethylacetamide (DMA) solution have been theoretically investigated. In DMA solution, the stable VO_2^+-containing complex is the four-coordinated $[V(O)_2(DMA)_2]^+$ species. For the gross reaction of 2HMF + O_2 → 2DFF + $2H_2O$, there are three main reaction stages, *i.e.*, the oxidation of the first HMF to DFF with the reduction of $[V(O)_2(DMA)_2]^+$ to $[V(OH)_2(DMA)]^+$, the aerobic oxidation of $[V(OH)_2(DMA)]^+$ to the peroxide $[V(O)_3(DMA)]^+$, and the oxidation of the second HMF to DFF with the reduction of $[V(O)_3(DMA)]^+$ to $[V(O)_2(DMA)_2]^+$. The rate-determining reaction step is associated with the C–H bond cleavage of $-CH_2$ group of the first HMF molecule. The peroxide $[V(O)_3(DMA)]^+$ species exhibits better oxidative activity than the initial $[V(O)_2(DMA)_2]^+$ species, which originates from its narrower HOMO–LUMO gap. The counteranion Cl^- exerts promotive effect on the aerobic oxidation of HMF to DFF catalyzed by $[V(O)_2(DMA)_2]^+$ species.

1. Introduction

Currently, 5-hydroxymethylfurfural (HMF), as an important platform for connecting biomass and petrochemical industry, has attracted wide attention, due to its sustainable production of high value-added chemicals, such as 2,5-diformylfuran (DFF).[1,2] DFF can be used as a multifunctional intermediate for the synthesis of pharmaceuticals and functional polymers.[3,4] Especially, DFF can be synthesized *via* a partial oxidation of the primary hydroxyl group without attacking reactive unsaturated aldehyde group from HMF, using clean O_2 as an oxidant.[5] At present, however, DFF is still commercially expensive and only available in milligram quantities.

In order to improve the yield of selective partial oxidation of HMF to DFF, deep oxidation of HMF must be avoided. Therefore, it is necessary to develop suitable catalytic oxidation system. To this end, various catalytic systems have been explored, including ruthenium-,[6–8] silver-,[9] copper- ,[10] iron-,[11] manganese-,[12,13] molybdenum-,[14–16] and vanadium-containing catalysts.[17–23,44] Particularly, V-containing catalysts have been proved to be good efficient and inexpensive. Unfortunately, the instability of HMF limits the application of pure HMF as the raw feedstock, because of the high cost of its downstream purification process. Encouragingly, for the scale synthesis of DFF, a promising approach is the direct production from cheap and accessible glucose, avoiding the separation of unstable HMF intermediate from solution.[23,24] Interestingly, our group have previously proposed one-pot-two-steps conversion of glucose into DFF, over both $CrCl_3$/NaBr catalyst for isomerization/dehydration and $NaVO_3$ catalyst for partial oxidation in *N*,*N*-dimethylacetamide (DMA) solution.[23] Herein, the experimental system includes the water produced from glucose and the Lewis acid Cr^{3+}, which make the solution acidic. Thereupon, when $NaVO_3$ can be readily dissolved in acidic DMA solution, the dissolved V-species may exist as VO_2^+ cation in acidic DMA solution.[25] Moreover, there are some counterpart anions of VO_2^+, *e.g.*, Cl^- and Br^-, in actually experimental DMA solution.[23]

[a]*College of Chemical Engineering, Sichuan University, Chengdu, Sichuan, 610065, P.R. China. E-mail: huaqingyang@scu.edu.cn; Fax: +86 28 85464466; Tel: +86 28 85464466*

[b]*Key Laboratory of Green Chemistry and Technology, Ministry of Education, College of Chemistry, Sichuan University, Chengdu, Sichuan, 610064, P.R. China*

† Electronic supplementary information (ESI) available: Sum of electronic energies, thermal correction to Gibbs free energy and relative Gibbs energies of various species. The MOL files of various species. Arrhenius plots of the calculated rate constants for the crucial reaction steps. See DOI: 10.1039/d1ra07297h

These counterpart anions may affect the catalytic performance of VO_2^+. Despite the present research achievement, the experimental study of direct synthesis of DFF from glucose still faces some problems, such as low yield of DFF, poor recycling of catalyst, and high cost of product separation and purification. To improve these issues, it is necessary to understand the relevant catalytic molecular mechanism.

In this study, we report a completely molecular mechanism for the aerobic oxidation of HMF to DFF catalyzed by VO_2^+ with Cl^- in DMA solution. The objectives are as following: (a) to ascertain the stable form of VO_2^+ and solvent DMA coordination, (b) to elucidate the detailed reaction pathways for the aerobic oxidation of HMF to DFF catalyzed by VO_2^+-containing complex, (c) to acquire the determining intermediate (DI) and the determining transition state (DTS), based on the energetic span,[26–29] (d) to gain the catalytic nature of VO_2^+ species, and (e) to obtain the effects of counterpart anions on the stabilization of both DI and DTS, which may engineer the novel design of green and efficient catalytic system toward the synthesis of DFF from HMF.

2. Computational details

In DMA media, all geometry calculations were performed with Gaussian 09 program.[30] To simulate the DMA solvent effect, a polarized continuum model based on solute electron density (PCM-SMD) was employed.[31,32] Full geometric optimizations were run to locate all stationary points, using M06 density functional theory method[33,34] with the 6-311++G(d, p) basis set[35,36] for the main-group elements (H, C, O, N, and Cl), and aug-cc-pVTZ basis set for the 3d transition metal (V) in view of relativistic effect,[37] namely, M06/6-311++G(d,p), aug-cc-pVTZ,. Each stationary point was characterized by harmonic vibrational frequency calculation (all real frequencies for intermediate and only one imaginary frequency for transition state), in which the zero-point energy (ZPE) was also gained. Each transition state structure was also verified by intrinsic reaction coordinate (IRC).[38,39] The natural atomic charges were analyzed, using the natural bond orbital (NBO) method.[40,41] Unless otherwise stated, the Gibbs free energy of formation (ΔG) are relative to the initial catalyst and reactants in DMA solution, under experimental temperature and pressure (383.0 K and 1.0 atm).[23]

Based on the energetic span model,[28] the rate-determining step was diagnosed, gaining the determining intermediate (DI) and the determining transition state (DTS). The rate constants were assessed over the 353–433 K temperature range, on the basis of conventional transition state theory, together with tunnelling correction, as described in our previous study.[42,43]

In DMA solution, DMA molecule coordinates readily to VO_2^+ species, forming $[V(O)_2(DMA)_x]^+$ complex. The Gibbs free energy of formation (ΔG) of each species $[V(O)_2(DMA)_x]^+$ starting from two independent species (VO_2^+ and DMA) was computed following the reaction

$$VO_2^+ + x(DMA) \rightarrow [V(O)_2(DMA)_x]^+ \quad (1)$$

And using the following the equation:

$$\Delta G = G_{[V(O)_2(DMA)_x]^+} - G_{VO_2^+} - xG_{DMA} \quad (2)$$

3. Results and discussion

For the reactant HMF molecules, as reported earlier,[43] there are eight possible conformers. For eight conformers of HMF in DMA solution, the geometric structures and relative Gibbs free energy are shown in Fig. S3† from ESI. As depicted in Fig. S3,† for the eight conformers of HMF, the relative Gibbs free energies increase as HMF-1 < HMF-2 < HMF-3 < HMF-6 < HMF-4 < HMF-8 < HMF-5 < HMF-7 in DMA solution. It is indicated that the conformer HMF-1 is thermodynamically the most stable in DMA solution.

Here, the ground state of O_2 molecule is the triplet state with the singlet state as the first excited state. The superscript prefixes "^{1}" and "^{3}" represents the singlet and triplet states, respectively. Unless specified, the default state is the ground state "^{1}".

For the product DFF molecules, there are three possible conformers. For three conformers of DFF in DMA solution, the geometric structures and relative Gibbs free energy are shown in Fig. S4† from ESI. As depicted in Fig. S4,† the relative Gibbs free energies increase as DFF-2 < DFF-3 < DFF-1. It is inferred that the conformer DFF-2 is thermodynamically the most preferable in DMA solution. Thereupon, the conformer HMF-1 is preferred as the initial reactant in the present study, while the conformer DFF-2 is regarded as the product.

For the aerobic of HMF to DFF, the following gross reaction will be studied:

$$2HMF + O_2 \rightarrow 2DFF + 2H_2O \quad (3)$$

The possible reaction pathways are depicted in Scheme 1, based on the relevant literatures.[15,16,44]

3.1 Stable coordination species of VO_2^+ with DMA

In DMA solution, the optimized geometric structures and the formed Gibbs free energies of $[V(O)_2(DMA)_x]^+$ complexes are shown in Fig. 1.

As depicted in Fig. 1, with regard to the DMA coordinating to V-site of VO_2^+, there are two coordination types, *i.e.*, through N-

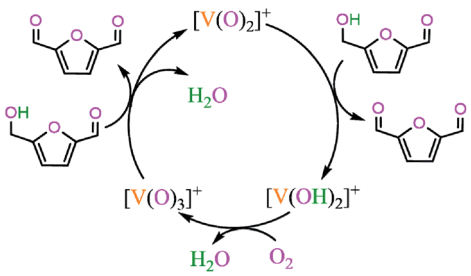

Scheme 1 Catalytic oxidation pathways of HMF to DFF.

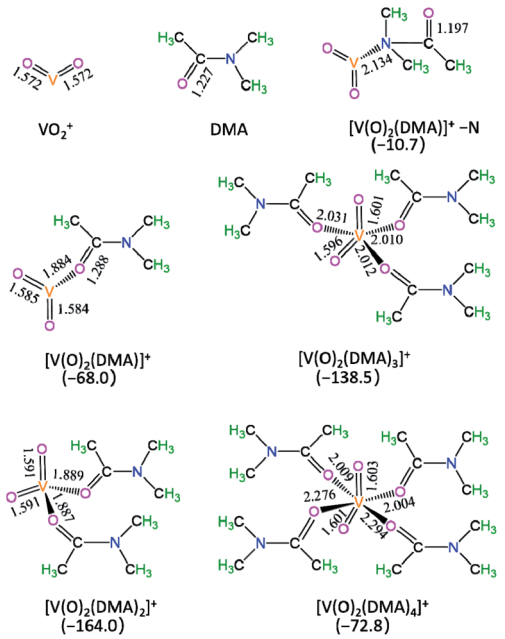

Fig. 1 The optimized geometric structures and the formed Gibbs free energies (G_r, kJ mol^{-1}) of $[V(O)_2(DMA)_x]^+$ complexes in the DMA solution. Bond lengths are reported in Å.

end and O-end of DMA, *i.e.*, $[V(O)_2(DMA)]^+$–N and $[V(O)_2(DMA)]^+$. For $[V(O)_2(DMA)]^+$–N and $[V(O)_2(DMA)]^+$, the ΔG value is −10.7 and −68.0 kJ mol^{-1}, respectively. It is inferred that the O-end coordination $[V(O)_2(DMA)]^+$ is 57.3 kJ mol^{-1} more stable than the N-end coordination $[V(O)_2(DMA)]^+$–N. That is to say, for the DMA coordination to V-site of VO_2^+, the O-end is stronger than the N-end.

Furthermore, for $[V(O)_2(DMA)_x]^+$ (x = 1–4) species, the ΔG value is −68.0, −164.0, −138.5, and −72.8 kJ mol^{-1}, respectively. It is obvious that the four-coordinated $[V(O)_2(DMA)_2]^+$ complex is thermodynamically the most preferable. Exceptionally, when the Cl^- anion interacts with VO_2^+, the corresponding complex $[V(O)_2(Cl)]$, with the stabilization energy of 147.8 kJ mol^{-1}, as shown in Table S1† from ESI. It is obvious that the $[V(O)_2(DMA)_2]^+$ complex is more 16.2 kJ mol^{-1} stable than the $[V(O)_2(Cl)]$ complex. Thereupon, the $[V(O)_2(DMA)_2]^+$ complex is preferred as the initial catalytic species.

3.2 $[V(O)_2(DMA)_2]^+ + HMF \rightarrow [V(OH)_2(DMA)]^+ + DFF + DMA$

The potential energy diagrams and geometric structures for the first HMF oxidation to DFF over $[V(O)_2(DMA)_2]^+$ cation without/with Cl^- anion are shown in Fig. 2, denoted as P-0-1 and P-Cl-1, respectively.

As depicted in Fig. 2, in the absence of counteranion Cl^-, there are four reaction steps, *i.e.*, (1) the formation of molecular complex 0-IM1 from the HMF-1 with exchanging with one DMA molecule from $[V(O)_2(DMA)_2]^+$, (2) the O–H bond cleavage *via* a four-membered cyclic 0-TS1 through addition unsaturated the first V=O double bond, (3) the C–H bond cleavage in –CH_2OH group *via* a five-membered 0-TS2 through addition unsaturated the second V=O double bond, resulting in the DFF formation, and (4) the release of DFF with leaving the reduced $[V(OH)_2(DMA)]^+$ behind.

The P-0-1 exhibits the energy height of the highest point (EHHP) of 196.9 kJ mol^{-1} at 0-TS2, the highest energy barrier (HEB) of 177.9 kJ mol^{-1} at the reaction step of 0-IM2 → 0-TS2 → 0-IM3, and the energy height of the lowest point (EHLP) of 0.0 kJ mol^{-1} at the initial point. The P-0-1 is concerned with the oxidation of the first HMF molecule to DFF, where the two V=O double bonds are reduced by addition to two V–OH group.

Additionally, in the presence of counteranion Cl^-, the P-Cl-1 is similar to P-0-1, there are differences in relative Gibbs free energies on the potential energy diagrams. The P-Cl-1 displays the EHHP of 186.4 kJ mol^{-1} at Cl-TS2, the HEB of 174.7 kJ mol^{-1} at the reaction step of Cl-IM2 → Cl-TS2 → Cl-IM3, and the EHLP of 0.0 kJ mol^{-1} at the initial point.

Compared with P-0-1, P-Cl-1 possesses lower EHHP (186.4 *vs.* 196.9 kJ mol^{-1}) and lower HEB (174.7 *vs.* 177.9 kJ mol^{-1}). It is indicated that the counteranion Cl^- exhibits some degree promotive effect for $[V(O)_2(DMA)_2]^+$ oxidizing the first HMF to DFF.

3.3 $[V(OH)_2(DMA)]^+ + O_2 \rightarrow [V(O)_3(DMA)]^+ + H_2O$

The potential energy diagrams and geometric structures for the oxidative dehydration of $[V(OH)_2(DMA)]^+$ to $[V(O)_3(DMA)]^+$ without/with Cl^- anion are shown in Fig. 3, denoted as P-0-2 and P-Cl-2, respectively.

As depicted in Fig. 3, in the absence of counteranion Cl^-, there are four reaction steps, *i.e.*, (1) the formation of molecular complex 0-IM5 between the interaction of O_2 with V-site of $[V(OH)_2(DMA)]^+$, (2) the O–H bond cleavage through [1,4]-H shift *via* a five-membered ring 0-TS3 for the formation of hydroxyl peroxide, (3) the cleavage of peroxide bond through [1,4]-H shift *via* a five-membered 0-TS4, leading to the H_2O formation, and (4) the release of H_2O molecule and saving the oxidized $[V(O)_3(DMA)]^+$ species. Particularly, although the ground state of O_2 is the triplet state, the triplet state ^{3}0-IM5 lies 60.4 kJ mol^{-1} above the singlet state 0-IM5. Thereby, a significant triplet–singlet spin inversion may occur once at 0-IM5. Here, for ^{3}0-IM5, the Mulliken spin densities are calculated to be 0.56 at O3, 0.48 at O4, and 0.99 at V. Moreover, for 0-IM5, the NBO analysis shows that the occupancies of V–O(3) and V–O(4) are 1.914 and 1.930*e*, respectively. It is indicated that the single bond of V–O(3) and V–O(4) have been formed. That is to say, in 0-IM5, the O_2 molecule is chemically adsorbed on V-site of $[V(OH)_2(DMA)]^+$.

The P-0-2 exhibits the EHHP of 168.6 kJ mol^{-1} at the initial point ($[V(OH)_2(DMA)]^+ + O_2$), the HEB of 124.8 kJ mol^{-1} at the reaction step of 0-IM5 → 0-TS3 → 0-IM6, and the EHLP of −40.6 kJ mol^{-1} at 0-IM5. Besides, the P-Cl-2 displays the EHHP of 170.3 kJ mol^{-1} at initial point ($[V(OH)_2(DMA)]^+\cdots Cl + O_2$), the HEB of 138.6 kJ mol^{-1} at the reaction step of Cl-IM5 → Cl-TS3 → Cl-IM6, and the EHLP of −57.2 kJ mol^{-1} at Cl-IM5.

Compared with P-0-2, P-Cl-2 includes lower EHLP (−57.2 *vs.* −40.6 kJ mol^{-1}). It is inferred that the counteranion Cl^- exhibits some degree stabilization effect toward 0-IM5.

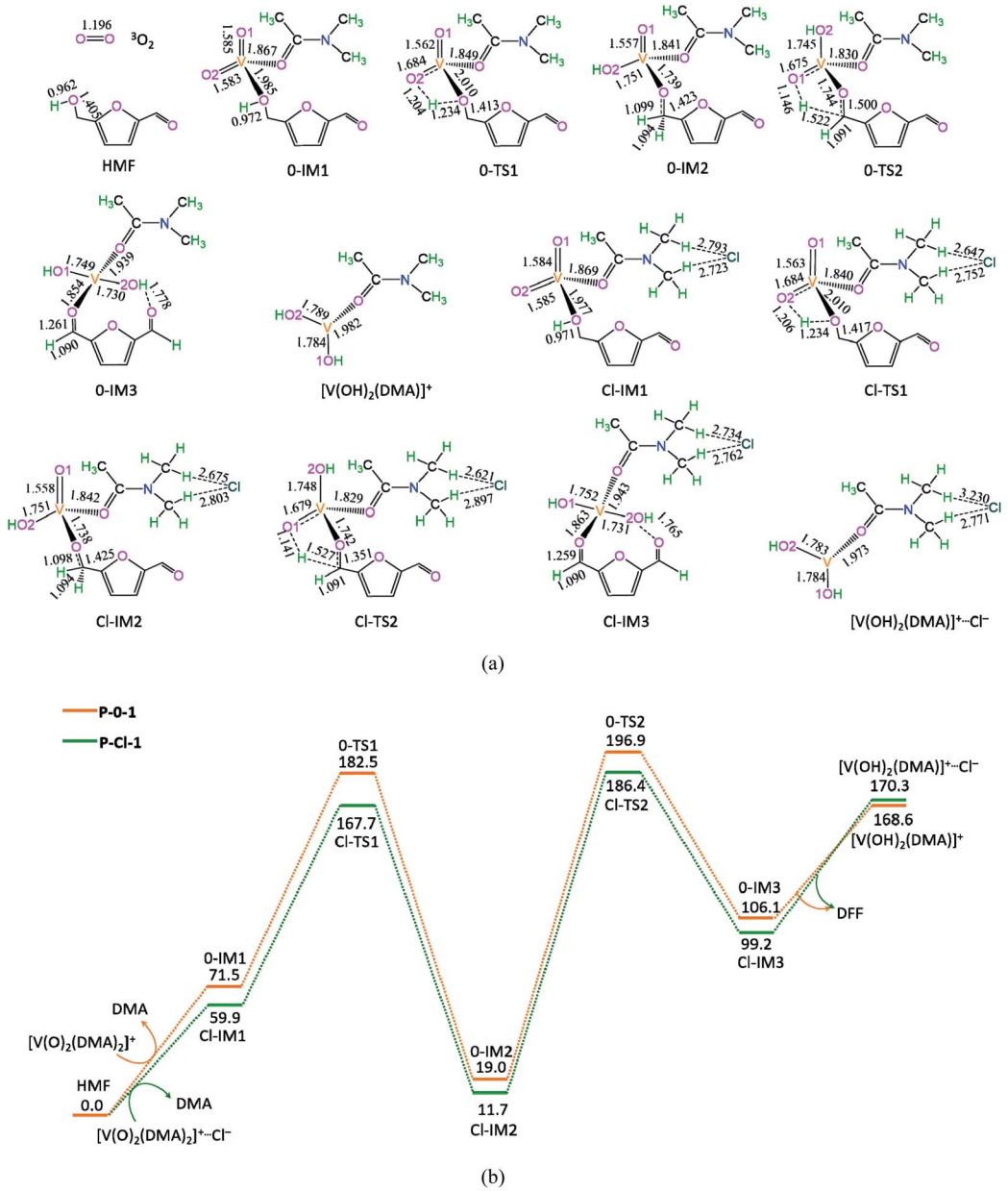

Fig. 2 The geometric structures (a) and the schematic energy diagrams (b) with the relative Gibbs free energy (G_r, kJ mol^{-1}) relative to the reactants for the first HMF oxidation to DFF catalyzed by $[V(O)_2(DMA)_2]^+$ without/with Cl^- in the DMA solution. For clarity, the hydrogen atoms on carbon are not shown. Bond lengths are reported in Å.

3.4 $[V(O)_3(DMA)]^+ + HMF + DMA \rightarrow [V(O)_2(DMA)_2]^+ + DFF + H_2O$

The potential energy diagrams and geometric structures for the oxidative dehydration of the second HMF to DFF by $[V(O)_3(DMA)]^+$ species without/with Cl^- anion are shown in Fig. 4, denoted as P-0-3 and P-Cl-3, respectively.

As depicted in Fig. 4, in the absence of counteranion Cl^-, there are seven reaction steps, *i.e.*, (1) the formation of a molecular complex 0-IM9 between the second HMF molecule and $[V(O)_3(DMA)]^+$ species through the O-end of –OH in HMF coordinating to V-site, (2) the O–H bond cleavage through [1,4]-H shift *via* a five-membered cyclic 0-TS5, (3) the C–H bond cleavage in $-CH_2OH$ group *via* a five-membered 0-TS6 through addition unsaturated V=O double bond for the DFF formation, (4) the release of DFF, saving the reduced $[V(OH)(OOH)(DMA)]^+$ aside, (5) $[V(OH)(OOH)(DMA)]^+$ readily rearranging to the isomer 0-IM13 with O–OH bond cleavage, (6) the O–H bond cleavage *via* a four-membered cyclic 0-TS7 through [1,3]-H shift for the H_2O formation, and (7) one DMA molecule exchanging with the H_2O molecule, regenerating the catalytic species $[V(O)_2(DMA)_2]^+$.

The P-0-3 displays the EHHP of 120.0 kJ mol^{-1} at 0-TS6, the HEB of 180.0 kJ mol^{-1} at the reaction step of 0-IM13 → 0-TS7 → 0-IM14, and the EHLP of −442.7 kJ mol^{-1} at 0-IM13. In

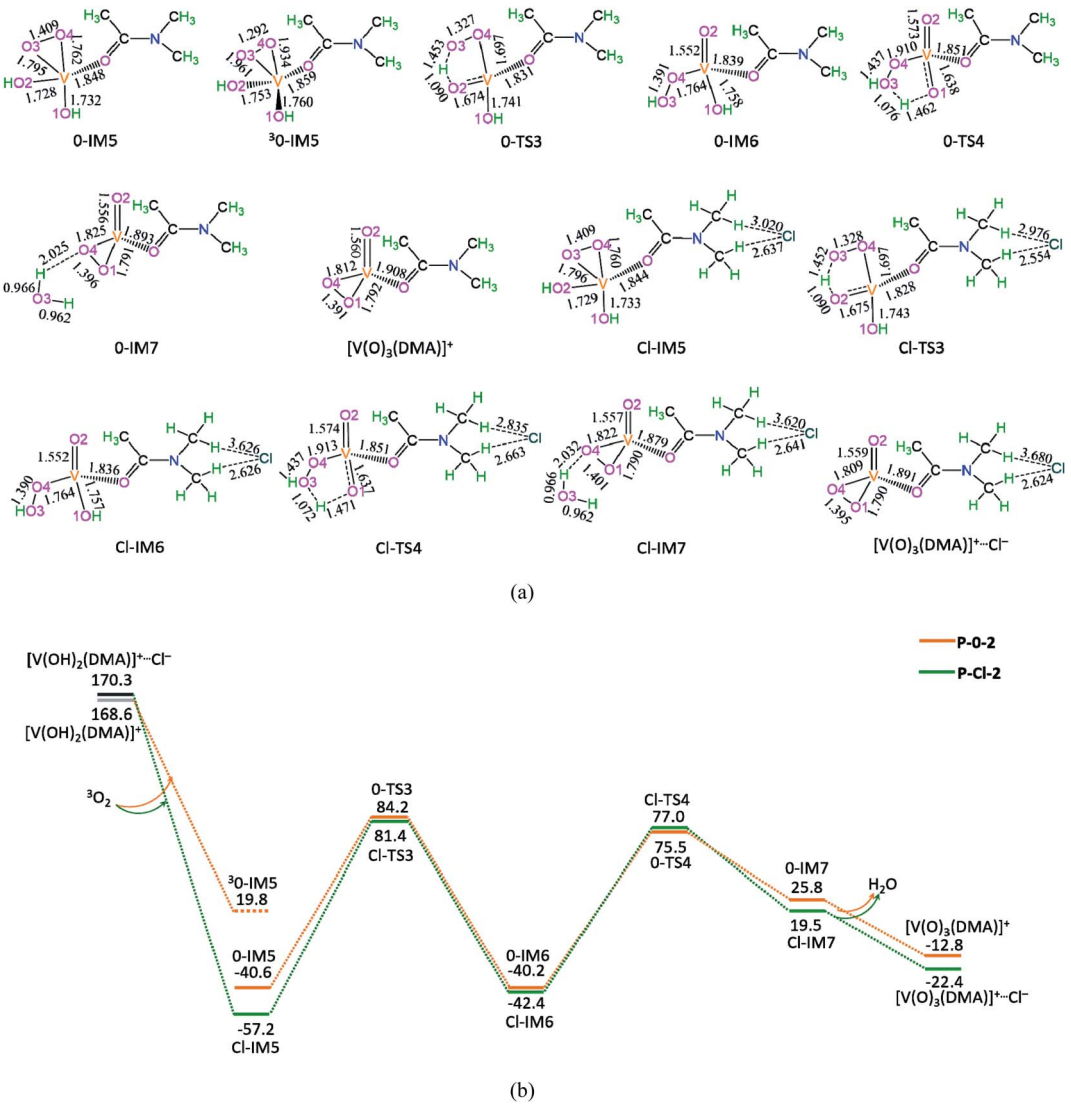

Fig. 3 The geometric structures (a) and the schematic energy diagrams (b) with the relative Gibbs free energy (G_r, kJ mol^{-1}) relative to the reactants for the oxidative dehydration of [V(OH)$_2$(DMA)]$^+$ to [V(O)$_3$(DMA)]$^+$ catalyzed by without/with Cl$^-$ in the DMA solution. For clarity, the hydrogen atoms on carbon are not shown. Bond lengths are reported in Å.

addition, the P-Cl-3 shows the EHHP of 92.7 kJ mol^{-1} at Cl-TS6, the HEB of 177.6 kJ mol^{-1} at the reaction step of Cl-IM13 → Cl-TS7 → Cl-IM14, and the EHLP of −459.7 kJ mol^{-1} at Cl-IM14.

Compared with P-0-3, P-Cl-3 involves lower EHHP (92.7 *vs.* 120.0 kJ mol^{-1}) and lower EHLP (−459.7 *vs.* −442.7 kJ mol^{-1}). It is indicated that counteranion Cl$^-$ stabilizes in some degree the relevant TS and IM.

3.5 Catalytic global analysis

As mentioned earlier, over [V(O)$_2$(DMA)$_2$]$^+$ species, the global catalytic cycle is made up of the reaction pathways of P-0-1, P-0-2, and P-0-3, denoted as G-0. Using energetic span model analysis, for G-0, the DI and DTS are computed to be the initial point ([V(O)$_2$(DMA)$_2$]$^+$ + HMF) and 0-TS2, respectively. The rate constants $k_{G\text{-}0}$ of ([V(O)$_2$(DMA)$_2$]$^+$ + HMF) → 0-TS2 (in s^{-1} mol^{-1} dm^3) can be expressed by the following formula:

$$k_{G\text{-}0} = 1.45 \times 10^8 \exp(-155\,949/RT) \quad (4)$$

Moreover, as mentioned earlier, the crucial reaction step is associated with the C–H bond cleavage of methylene group in HMF. Here, the [V(O)$_2$(DMA)$_2$]$^+$ species exerts oxidative effect for the first HMF oxidation to DFF, while the peroxide [V(O)$_3$(DMA)]$^+$ species behaves as an oxidant for the second HMF oxidation to DFF. The peroxide [V(O)$_3$(DMA)]$^+$ species exhibits higher oxidative activity than the [V(O)$_2$(DMA)$_2$]$^+$ species, toward the C–H bond cleavage of methylene group in HMF. For [V(O)$_2$(DMA)$_2$]$^+$ and [V(O)$_3$(DMA)]$^+$ species, the LUMO and HOMO molecular orbitals are shown in Fig. 5. The LUMO–HOMO gaps are 5.49 and 3.66 eV for [V(O)$_2$(DMA)$_2$]$^+$ and [V(O)$_3$(DMA)]$^+$, respectively. It is obvious that LUMO–HOMO gap for [V(O)$_3$(DMA)]$^+$ is narrower than that for [V(O)$_2$(DMA)$_2$]$^+$. Moreover, the positions of LUMO are relatively concentrated in V–O–O region for [V(O)$_3$(DMA)]$^+$, and in O–V–O region for

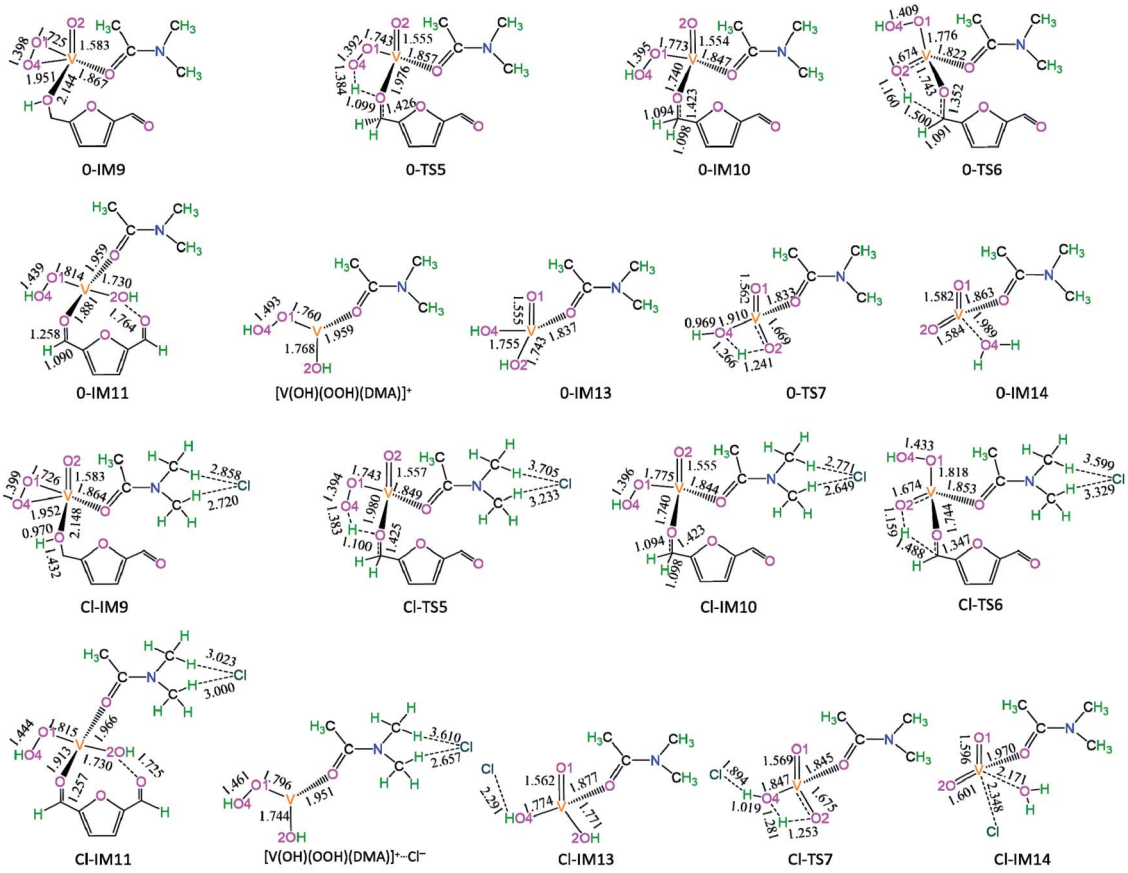

(a)

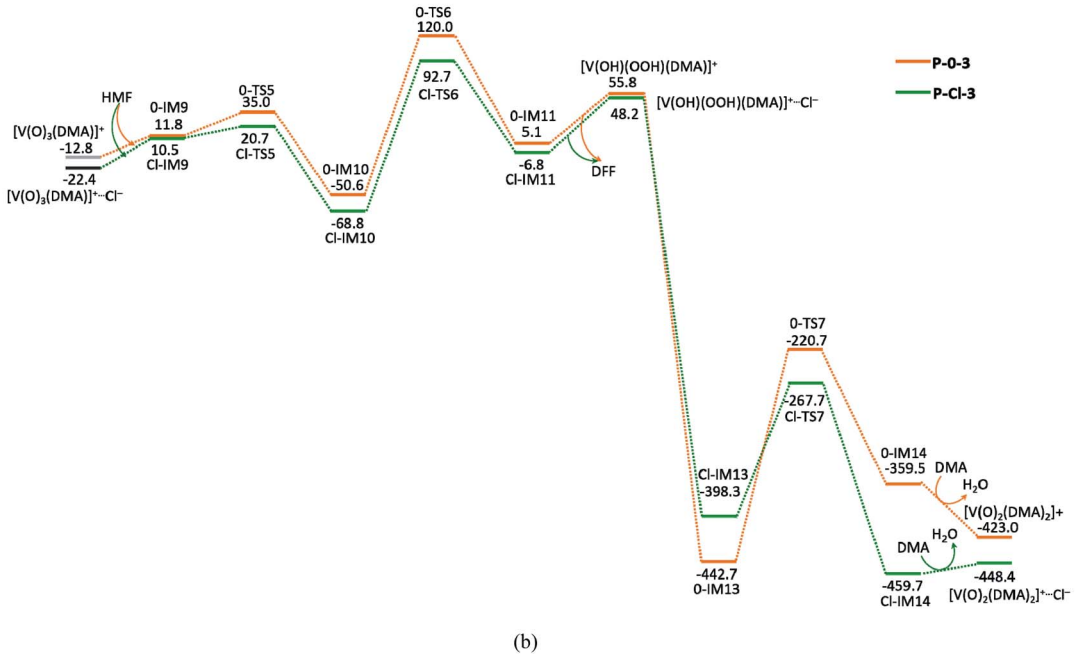

(b)

Fig. 4 The geometric structures (a) and the schematic energy diagrams (b) with the relative Gibbs free energy (G_r, kJ mol^{-1}) relative to the reactants for the oxidative dehydration of the second HMF to DFF by $[V(O)_3(DMA)]^+$ without/with Cl^- in the DMA solution. For clarity, the hydrogen atoms on carbon are not shown. Bond lengths are reported in Å.

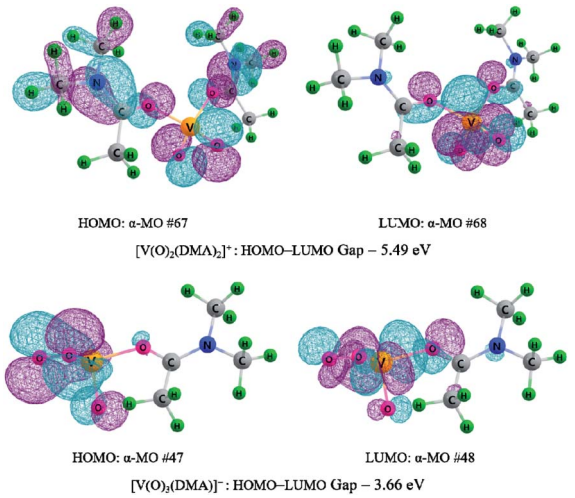

Fig. 5 Highest occupied molecular orbital (HOMO), lowest unoccupied molecular orbital (LUMO) and the HOMO–LUMO energy gap for $[V(O)_2(DMA)_2]^+$ and $[V(O)_3(DMA)]^+$. The orbital contour value was 0.03.

$[V(O)_2(DMA)_2]^+$. The V–O–O peroxy functional group in $[V(O)_3(DMA)]^+$ shows stronger oxidation than the V–O functional group in $[V(O)_2(DMA)_2]^+$. Thereupon, $[V(O)_3(DMA)]^+$ displays a higher oxidizability than $[V(O)_2(DMA)_2]^+$, toward the C–H bond cleavage in the methylene group in HMF.

In the presence of counteranion Cl^-, *i.e.*, over $[V(O)_2(DMA)_2]^+\cdots Cl^-$, the global catalytic cycle is composed of P-Cl-1, P-Cl-2, and P-Cl-3, denoted as G-Cl. For G-Cl, the DI and DTS are acquired to be initial point ($[V(O)_2(DMA)_2]^+\cdots Cl$ + HMF) and Cl-TS2. The rate constants $k_{G\text{-}Cl}$ of ($[V(O)_2(DMA)_2]^+\cdots Cl^-$ + HMF) → Cl-TS2 (in s^{-1} mol^{-1} dm^3) can be expressed by the following formula:

$$k_{G\text{-}Cl} = 2.74 \times 10^8 \exp(-155\,189/RT) \quad (5)$$

The rate constant of $k_{G\text{-}Cl}$ is 1.5–1.3 times larger than that of $k_{G\text{-}0}$, over the 353–433 K temperature range. This result echoes that the counteranion Cl^- promotes the catalytic activity of $[V(O)_2(DMA)_2]^+$ toward the aerobic oxidation of HMF to DFF.

4. Conclusions

The aerobic oxidation mechanism of HMF to DFF catalyzed by VO_2^+ with counterpart anion in DMA solution have been theoretically studied. The following conclusions can be drawn from the present results.

In DMA solution, the stable VO_2^+-containing complex is the four-coordinated $[V(O)_2(DMA)_2]^+$ species. For the gross reaction of 2HMF + O_2 → 2DFF + $2H_2O$, there are three main reaction stages, *i.e.*, the oxidation of the first HMF to DFF with the reduction of $[V(O)_2(DMA)_2]^+$ to $[V(OH)_2(DMA)]^+$, the aerobic oxidation of $[V(OH)_2(DMA)]^+$ to the peroxide $[V(O)_3(DMA)]^+$, and the oxidation of the second HMF to DFF with the reduction of $[V(O)_3(DMA)]^+$ to $[V(O)_2(DMA)_2]^+$. The initial $[V(O)_2(DMA)_2]^+$ species is responsible for the oxidation of the first HMF, while the peroxide $[V(O)_3(DMA)]^+$ species is in charge of the oxidation of the second HMF. The rate-determining reaction step is concerned with the C–H bond cleavage of $-CH_2$ group of the first HMF molecule. The peroxide $[V(O)_3(DMA)]^+$ species shows better oxidative activity than the initial $[V(O)_2(DMA)_2]^+$ species, which stems from its narrower HOMO–LUMO gap. The counteranion Cl^- displays promotive effect on the catalytic activity of $[V(O)_2(DMA)_2]^+$ species, toward the aerobic oxidation of HMF to DFF.

Conflicts of interest

There are no conflicts to declare.

Acknowledgements

The authors are grateful for financial support by the National Natural Science Foundation of China (No: 22073064 and 21573154) and the 111 Project (B17030).

Notes and references

1 P. Priyanka and S. Shunmugavel, *ChemSusChem*, 2019, **12**, 145–163.
2 X. Kong, Y. Zhu, Z. Fang, J. A. Kozinski, I. S. Butler, L. Xu, H. Song and X. Wei, *Green Chem.*, 2018, **20**, 3657–3682.
3 J. Mitra, X. Zhou and T. Rauchfuss, *Green Chem.*, 2015, **17**, 307–313.
4 Y. Xu, X. Jia, J. Ma, J. Gao, F. Xia, X. Li and J. Xu, *Green Chem.*, 2018, **20**, 2697–2701.
5 F. W. Lichtenthaler, *Acc. Chem. Res.*, 2002, **35**, 728–737.
6 C. A. Antonyraj, J. Jeong, B. Kim, S. Shin, S. Kim, K. Lee and J. K. Cho, *J. Ind. Eng. Chem.*, 2013, **19**, 1056–1059.
7 Y. Wang, B. Liu, K. Huang and Z. Zhang, *Ind. Eng. Chem. Res.*, 2014, **53**, 1313–1319.
8 J. Nie, J. Xie and H. Liu, *J. Catal.*, 2013, **301**, 83–91.
9 G. D. Yadav and R. V. Sharma, *Appl. Catal., B*, 2014, **147**, 293–301.
10 W. Zhang, J. Xie, W. Hou, Y. Liu, Y. Zhou and J. Wang, *ACS Appl. Mater. Interfaces*, 2016, **8**, 23122–23132.
11 B. Liu, Z. Zhang, K. Lv, K. Deng and H. Duan, *Appl. Catal., A*, 2014, **472**, 64–71.
12 J. Nie and H. Liu, *J. Catal.*, 2014, **316**, 57–66.
13 Y. Yao and G. Wang, *J. Phys. Chem. C*, 2021, **125**, 3818–3826.
14 Y. Liu, L. Zhu, J. Tang, M. Liu, R. Cheng and C. Hu, *ChemSusChem*, 2014, **7**, 3541–3547.
15 L. Ren, H. Yang and C. Hu, *Catal. Sci. Technol.*, 2016, **6**, 3776–3787.
16 Z. Wang, L. Liu, B. Xiang, Y. Wang, Y. Lyu, T. Qi, Z. Si, H. Yang and C. Hu, *Catal. Sci. Technol.*, 2019, **9**, 811–821.
17 W. Zhang, T. Meng, J. Tang, W. Zhuang, Y. Zhou and J. Wang, *ACS Sustainable Chem. Eng.*, 2017, **5**, 10029–10037.
18 W. Hou, Q. Wang, Z. Guo, J. Li, Y. Zhou and J. Wang, *Catal. Sci. Technol.*, 2017, **7**, 1006.
19 Y. Zhou, Z. Ma, J. Tang, N. Yan, Y. Du, S. Xi, K. Wang, W. Zhang, H. Wen and J. Wang, *Nat. Commun.*, 2018, **9**, 2931.
20 I. Sádaba, Y. Y. Gorbanev, S. Kegnaes, S. S. R. Putluru, R. W. Berg and A. Riisager, *ChemCatChem*, 2013, **5**, 284–293.

21 J. Nie and H. Liu, *Pure Appl. Chem.*, 2012, **84**, 765–777.
22 N. T. Le, P. Lakshmanan, K. Cho, Y. Han and H. Kim, *Appl. Catal., A*, 2013, **464–465**, 305–312.
23 X. Xiang, L. He, Y. Yang, B. Guo, D. Tong and C. Hu, *Catal. Lett.*, 2011, **141**, 735–741.
24 A. Takagaki, M. Takahashi, S. Nishimura and K. Ebitani, *ACS Catal.*, 2011, **1**, 1562–1565.
25 L. F. Zhu, B. Guo, D. Y. Tang, X. K. Hu, G. Y. Li and C. W. Hu, *J. Catal.*, 2007, **245**, 446–455.
26 A. Uhe, S. Kozuch and S. Shaik, *J. Comput. Chem.*, 2011, **32**, 978–985.
27 S. Kozuch and S. Shaik, *Acc. Chem. Res.*, 2011, **44**, 101–110.
28 S. Kozuch, *ACS Catal.*, 2015, **5**, 5242–5255.
29 W. Wang and G. Wang, *RSC Adv.*, 2015, **5**, 83459–83470.
30 M. J. Frisch, G. W. Trucks, H. B. Schlegel, G. E. Scuseria, M. A. Robb, J. R. Cheeseman, G. Scalmani, V. Barone, B. Mennucci and G. A. Petersson, *et al.*, *Revision C.01*, Gaussian, Inc, Wallingford, CT, 2010.
31 A. V. Marenich, C. J. Cramer and D. G. Truhlar, *J. Phys. Chem. B*, 2009, **113**, 6378–6396.
32 M. Cossi, G. Scalmani, N. Rega, V. Barone, *et al.*, *J. Chem. Phys.*, 2002, **117**, 43–54.
33 Y. Zhao and D. G. Truhlar, *Theor. Chem. Acc.*, 2008, **120**, 215–241.
34 Y. Zhao and D. G. Truhlar, *Acc. Chem. Res.*, 2008, **41**, 157–167.
35 R. Krishnan, J. S. Binkley, R. Seeger, J. A. Pople, *et al.*, *J. Chem. Phys.*, 1980, **72**, 650–654.
36 A. D. McLean and G. S. Chandler, *J. Chem. Phys.*, 1980, **72**, 5639–5648.
37 N. B. Balabanov and K. A. Peterson, *J. Chem. Phys.*, 2005, **123**, 64107.
38 R. Bauernschmitt and R. Ahlrichs, *J. Chem. Phys.*, 1996, **104**, 9047–9052.
39 C. Gonzalez and H. B. Schlegel, *J. Phys. Chem.*, 1990, **94**, 5523–5527.
40 A. E. Reed, R. B. Weinstock and F. Weinhold, *J. Chem. Phys.*, 1985, **83**, 735–746.
41 A. E. Reed, L. A. Curtiss and F. Weinhold, *Chem. Rev.*, 1988, **88**, 899–926.
42 B. Xiang, Y. Wang, T. Qi, H. Yang and C. Hu, *J. Catal.*, 2017, **352**, 586–598.
43 L. Ren, L. Zhu, T. Qi, J. Tang, H. Yang and C. Hu, *ACS Catal.*, 2017, **7**, 2199–2212.
44 L. Liu, Z. Wang, Y. Lyu, J. Zhang, Z. Huang, T. Qi, Z. Si, H. Yang and C. Hu, *Catal. Sci. Technol.*, 2020, **10**, 278–290.